Proton Transfer Tautomerization in *N*-Salicylideneanilines upon Charge-Transfer Complex Formation. 7,7,8,8-Tetracyanoquinodimethane (TCNQ) and 2,3,5,6-Tetrafluoro-7,7,8,8-tetracyanoquinodimethane (F_4TCNQ) Complexes of *N*-(2-Hydroxy-1-naphthylmethylene)-1-pyrenamine and *N*,*N*′-Bis(2-hydroxy-1-naphthylmethylene)-*p*-phenylenediamine

Tamotsu INABE,* Naomi HOSHINO-MIYAJIMA, Isabelle LUNEAU,†,# Tadaoki MITANI,††,## and Yusei MARUYAMA†

Department of Chemistry, Faculty of Science, Hokkaido University, Sapporo 060
†Institute for Molecular Science, Myodaiji, Okazaki 444

(Received August 11, 1993)

TCNQ and F_4TCNQ complexes of *N*-(2-hydroxy-1-naphthylmethylene)aniline-type compounds, *N*-(2-hydroxy-1-naphthylmethylene)-1-pyrenamine (NPY) and *N*,*N*′-bis(2-hydroxy-1-naphthylmethylene)-*p*-phenylenediamine (DNP) have been prepared and subjected to structural and optical studies in the crystalline state. An X-ray crystallographic study indicates that the donors and acceptors are mixed along a one-dimensional column in all complexes. The intramolecular O–H···N hydrogen bond structure is sensitively changed upon complex formation; the hydrogen atom is located at the nitrogen site in TCNQ complexes and shifts to the center of the hydrogen bond in F_4TCNQ complexes. The hydrogen-bond structure is found to vary with some correlation to the strength of the charge-transfer interaction.

In our preceding paper[1] we showed that the intramolecular hydrogen-bond structure in *N*-(2-hydroxy-1-naphthylmethylene)aniline-type compounds is an average of O–H···N and O···H–N. From an NMR study, it has been confirmed that the dynamic motion of the proton is the origin of this hydrogen-bond structure. These results suggest that the potential of the proton in the hydrogen bond is rather close to a symmetrical double-well with a small energy barrier.

We are also interested in these derivatives from a diferent point of view. By substituting 2-hydroxyphenyl in the *N*-salicylideneaniline framework to 2-hydroxy-1-naphthyl, the ionization potential is expected to become smaller. In fact, we have found that the electrochemical oxidation potentials of some *N*-salicylideneaniline derivatives decrease by 0.1—0.2 V upon this substitution. These derivatives are expected to form charge-transfer complexes with some acceptor molecules. Since the proton transfer in *N*-salicylideneanilines is accompanied by a configurational change of the π-electron structure, the electronic properties, such as electrical conductivity, are expected to be modulated by the proton motion or concertedly coupled with the proton motion when the intermolecular interaction is sufficiently strong. As we have shown before,[2] a hydrogen-bonded system with a charge-transfer interaction can be utilized for designing novel molecular devices based on such electron–proton coupling.

In this paper we show the structural and optical properties of charge-transfer complexes of *N*-(2-hydroxy-1-naphthylmethylene)-1-pyrenamine (NPY) and *N*,*N*′-bis(2-hydroxy-1-naphthylmethylene)-*p*-phenylenediamine (DNP). They are found to be electrically nonconducting, since the donors and acceptors are mixed-stacked. A combination of the structural and optical results, however, indicates an interesting correlation between the charge-transfer interaction and the hydrogen-bond structure.

Experimental

Materials. NPY and DNP were prepared by the same method as reported in a preceding paper.[1] TCNQ and F_4TCNQ were commercially obtained, and were purified by either recrystallization or vacuum sublimation. The NPY complexes were prepared by mixing NPY in a hot acetonitrile solution and TCNQ or F_4TCNQ in the same solvent. Single crystals of NPY–TCNQ and $(NPY)_2F_4TCNQ$ were obtained by slow evaporation of the saturated acetonitrile solutions with small crystals as seeds. The DNP complexes were similarly obtained using chlorobenzene as a solvent.

Measurements. The infrared absorption spectra of single-crystal specimens were measured using previously reported methods[3] and a Perkin–Elmer 1650 FT-IR microscope system. The visible and near-infrared absorption spectra were measured using a JASCO Ubest V-570 spectrometer.

X-Ray Structural Analyses. Automated Rigaku AFC-5R (NPY–TCNQ, $(NPY)_2F_4TCNQ$, and DNP–F_4TCNQ) and ENRAF NONIUS CAD4 (DNP–TCNQ) diffractometers with graphite monochromatized Mo $K\alpha$ radiation ($\lambda=0.71073$ Å) were used for data collection at room temperature. The data-collection conditions are summarized in Table 1. In all cases, the intensity data were collected over the range $2\theta<60°$ in the θ–2θ mode with a scan width of $(1.2+0.5\tan\theta)°$. Three standard reflections

#Present address: Liesg, Enseeg, Domaine Universitaire BP75, 38402 Saint-Martin D'Heres, France.
##Present address: Japan Advanced Institute of Science and Technology Hokuriku, Tatsunokuchi, Nomi, Ishikawa 923-12.

Table 1. Data-Collection Conditions and Crystal Data

	NPY-TCNQ	$(NPY)_2F_4TCNQ$	DNP-TCNQ	DNP-F_4TCNQ
Range of h,k, and l	$-15\leq h\leq 15$ $-25\leq k\leq 24$ $0\leq l\leq 11$	$-12\leq h\leq 12$ $-17\leq k\leq 16$ $0\leq l\leq 9$	$-14\leq h\leq 14$ $-14\leq k\leq 14$ $0\leq l\leq 11$	$-14\leq h\leq 14$ $-15\leq k\leq 15$ $0\leq l\leq 11$
Scan rate/° min−1	5	4	(auto)	8
Number of reflections measured	8915	4449	4793	4927
Number of independent reflections observed ($F_o>3\sigma$ (F_o))	4981	2132	2594	1634
Lattice parameter measurement				
2θ range/°	$25 < 2\theta < 30$	$21 < 2\theta < 30$	$23 < 2\theta < 30$	$22 < 2\theta < 30$
Number of reflections	50	50	25	50
Chemical formula	$C_{39}H_{21}N_5O$	$C_{66}H_{34}F_4N_6O_2$	$C_{40}H_{24}N_6O_2$	$C_{40}H_{20}F_4N_6O_4$
Molecular weight	575.6	1018.9	620.7	724.6
Crystal color	Black	Black	Black	Black
Crystal size/mm	0.55 × 0.40 × 0.20	0.60 × 0.20 × 0.04	0.35 × 0.20 ×0.10	0.55 × 0.13 × 0.10
Space group	$P\bar{1}$	$P\bar{1}$	$P\bar{1}$	$P\bar{1}$
a/Å	11.131(2)	10.836(2)	10.221(3)	10.079(2)
b/Å	17.804(3)	14.294(3)	10.342(2)	10.377(2)
c/Å	8.151(1)	8.076(2)	7.829(2)	8.013(2)
α/°	100.68(1)	106.86(2)	102.96(1)	104.38(1)
β/°	90.14(1)	101.52(2)	103.25(1)	100.74(2)
γ/°	115.23(1)	91.75(2)	95.87(1)	93.57(2)
V/Å^3	1429.8(4)	1167.8(5)	774.7(4)	792.4(3)
Z	2	1	1	1
D_c/g cm^{-3}	1.337	1.449	1.330	1.518
μ(Mo Kα)/cm^{-1}	0.77	0.94	0.79	1.10
R	0.059	0.037	0.068	0.043
R_w	0.056	0.040	0.059	0.045
Weighting factor(g) $w^{-1}=\sigma^2+(gF)^2$	0.015	0.015	0.015	0.015

monitored every 100 data measurements (every two hours for DNP–TCNQ) showed no significant deviation of intensities; the deviations were within 1.5% for NPY–TCNQ and $(NPY)_2F_4TCNQ$, within 1.6% for DNP–TCNQ, and within 1.3% for DNP–F_4TCNQ.

The crystals structures were solved by a direct method,[4] and the positions of all the hydrogen atoms were determined from difference synthesis maps. A block-diagonal least-squares technique (UNICS III[5]) with anisotropic thermal parameters for non-hydrogen atoms and isotropic for hydrogen atoms was employed for the structure refinements.

Results and Discussion

Molecular and Crystal Structures of the NPY Complexes. The atomic parameters obtained by an X-ray analysis for NPY–TCNQ are listed in Table 2.[6] The atom numbering scheme for NPY is the same as that for a single-component crystal.[1] The molecular structure of TCNQ with the bond lengths is shown in Fig. 1(a). The bond lengths for NPY are listed in Table 4 together with those in the F_4TCNQ complexes and those in the single-component crystal. The NPY molecule is nearly planar and practically the same as that in the single-component crystal; the dihedral angle between the naphthalene and pyrene rings is 5.9° in the TCNQ complex (5.9° in the NPY crystal at 295 K).

The most noticeable change upon complex formation

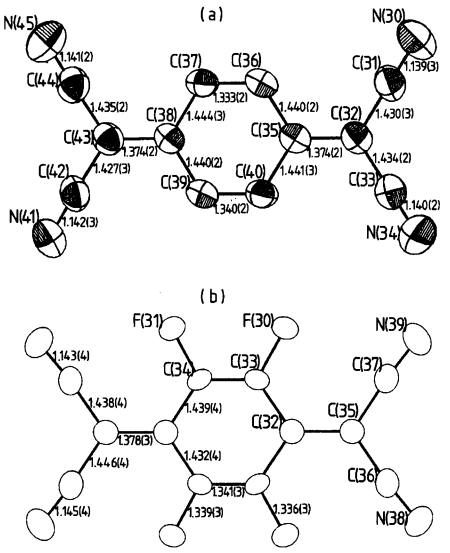

Fig. 1. ORTEP drawing and bond lengths (Å) of TCNQ in NPY–TCNQ (a) and F_4TCNQ in $(NPY)_2F_4TCNQ$.

appears in the hydrogen-bond structure. It has already been found that the CO distance in NPY is somewhat short as a normal hydroxyl group in the single-component crystal.[1] The CO distance is even shorter in NPY–TCNQ (1.292(2) Å). This length suggests that the pro-

Table 2. Fractional Coordinates ($\times 10^4$) and Equivalent Temperature Factors for NPY–TCNQ

Atom	x	y	z	B_{eq}/Å$^{2a)}$
O(1)	1728(1)	3019(1)	7634(1)	5.1(1)
C(2)	548(1)	2272(1)	4958(2)	3.5(1)
C(3)	896(2)	2321(1)	6672(2)	4.1(1)
C(4)	290(2)	1577(1)	7360(2)	5.6(1)
C(5)	−600(2)	843(1)	6405(3)	6.4(1)
C(6)	−986(2)	765(1)	4699(2)	5.1(1)
C(7)	−1954(2)	0(1)	3743(3)	7.4(1)
C(8)	−2340(2)	−80(1)	2116(3)	7.3(1)
C(9)	−1763(2)	612(1)	1371(3)	6.3(1)
C(10)	−819(2)	1374(1)	2262(2)	5.0(1)
C(11)	−407(2)	1477(1)	3949(2)	3.9(1)
C(12)	1146(2)	3008(1)	4280(2)	3.7(1)
N(13)	2006(1)	3737(1)	5189(2)	3.7(1)
C(14)	2658(1)	4506(1)	4639(2)	3.5(1)
C(15)	2333(2)	4600(1)	3064(2)	4.3(1)
C(16)	3000(2)	5352(1)	2549(2)	4.4(1)
C(17)	4018(2)	6046(1)	3581(2)	3.7(1)
C(18)	4734(2)	6840(1)	3076(2)	4.6(1)
C(19)	5693(2)	7504(1)	4104(2)	4.9(1)
C(20)	6059(2)	7461(1)	5752(2)	4.1(1)
C(21)	7048(2)	8144(1)	6865(3)	5.0(1)
C(22)	7382(2)	8072(1)	8433(3)	5.3(1)
C(23)	6738(2)	7314(1)	8965(2)	4.7(1)
C(24)	5723(2)	6615(1)	7921(2)	3.8(1)
C(25)	5019(2)	5822(1)	8426(2)	4.2(1)
C(26)	4045(2)	5149(1)	7406(2)	3.9(1)
C(27)	3667(1)	5194(1)	5756(2)	3.2(1)
C(28)	4350(1)	5971(1)	5207(2)	3.3(1)
C(29)	5376(1)	6680(1)	6297(2)	3.5(1)
N(30)	4349(2)	−1986(1)	347(2)	7.0(1)
C(31)	4290(2)	−1758(1)	854(2)	4.9(1)
C(32)	4209(2)	−1472(1)	−2360(2)	4.3(1)
C(33)	5136(2)	−616(1)	−2381(2)	5.2(1)
N(34)	5889(2)	59(1)	−2416(2)	7.8(1)
C(35)	3315(2)	−1993(1)	−3709(2)	3.8(1)
C(36)	2440(2)	−2861(1)	−3672(2)	4.0(1)
C(37)	1593(2)	−3375(1)	−4992(2)	4.1(1)
C(38)	1511(2)	−3077(1)	−6502(2)	3.7(1)
C(39)	2373(2)	−2204(1)	−6522(2)	4.0(1)
C(40)	3232(2)	−1688(1)	−5203(2)	4.1(1)
N(41)	497(2)	−3055(1)	−10527(2)	6.3(1)
C(42)	555(2)	−3306(1)	−9352(2)	4.8(1)
C(43)	648(2)	−3605(1)	−7871(2)	4.2(1)
C(44)	−222(2)	−4478(1)	−7896(2)	4.9(1)
N(45)	−904(2)	−5172(1)	−7903(2)	6.9(1)

a) $B_{eq}=4/3\sum_i\sum_j \beta_{ij} a_i a_j$.

ton is completely transferred to the nitrogen site (vide infra).

The crystal sturcture is shown in Fig. 2. The donors and acceptors are mixed along the stacking direction. The repeating unit is $(TCNQ)_2$–NPY–NPY, and there are inversion centers between the acceptors and between the donors. Molecular overlaps are shown in Fig. 3. The interplanar distances are 3.42 Å between the naphthalene ring and TCNQ, 3.42 Å between the pyrene ring and TCNQ, and 3.47 Å between the pyrene rings.

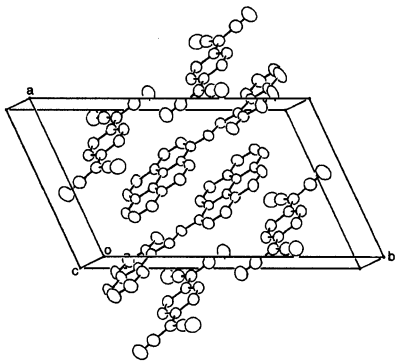

Fig. 2. Crystal structure of NPY–TCNQ.

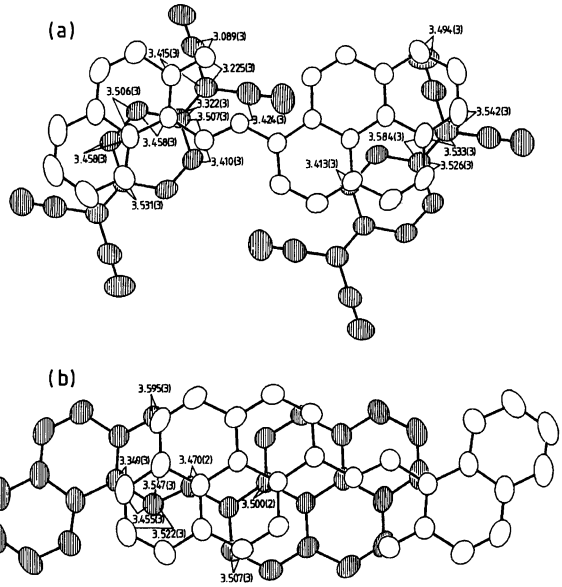

Fig. 3. Molecular overlaps between TCNQ and NPY (a) and NPY and NPY (b) in NPY–TCNQ with short interatomic distances (Å).

Since the rings are not perfectly parallel, except for the pyrene rings, the values are only nominal; the distances given are between the mean plane and the center of the ring. In fact, there are shorter interatomic distances between the naphthalene ring and TCNQ than between the pyrene ring and TCNQ. It may be more precise to say that the repeat unit is a combination of two TCNQ–NPY related by an inversion center, since there are much fewer interactions between the NPY molecules.

The degree of charge transfer can be estimated from the geometry of TCNQ following an empirical equation proposed by Kistenmacher et al.[7] The estimated value is less than 0.1. Since the ionization potential of the donor is not very small (the first oxidation potential is about 1.0 V vs. Ag·AgCl in acetonitrile), it is quite reasonable that the ground state is nearly neutral.

The reaction between NPY and F_4TCNQ gave a 2:1 complex. The structure of F_4TCNQ in this complex is shown in Fig. 1(b), and the atomic parameters are given in Table 3.[6] The atom numbering scheme of NPY is

Table 3. Fractional Coordinates ($\times 10^4$) and Equivalent Temperature Factors for $(NPY)_2F_4TCNQ$

Atom	x	y	z	B_{eq}/Å$^{2a)}$
O(1)	2905(2)	2066(1)	14034(2)	4.2(1)
C(2)	2341(2)	2942(2)	11921(3)	2.9(1)
C(3)	2561(3)	2874(2)	13671(3)	3.3(1)
C(4)	2407(3)	3691(2)	15098(3)	4.2(1)
C(5)	2071(3)	4542(2)	14805(4)	4.3(1)
C(6)	1885(3)	4666(2)	13077(4)	3.5(1)
C(7)	1603(3)	5577(2)	12819(4)	4.4(1)
C(8)	1496(3)	5713(2)	11194(4)	5.2(1)
C(9)	1621(3)	4924(2)	9750(4)	4.9(1)
C(10)	1852(3)	4020(2)	9950(4)	4.1(1)
C(11)	2013(2)	3866(2)	11617(3)	3.0(1)
C(12)	2468(3)	2114(2)	10509(3)	3.2(1)
N(13)	2786(2)	1288(1)	10806(3)	3.0(1)
C(14)	2946(2)	431(2)	9499(3)	2.7(1)
C(15)	2581(3)	310(2)	7678(3)	3.2(1)
C(16)	2732(2)	−562(2)	6455(3)	3.2(1)
C(17)	3256(2)	−1338(2)	6993(3)	2.9(1)
C(18)	3445(3)	−2238(2)	5746(3)	3.6(1)
C(19)	3945(3)	−2978(2)	6287(4)	3.8(1)
C(20)	4289(2)	−2908(2)	8131(4)	3.4(1)
C(21)	4774(3)	−3682(2)	8709(4)	4.1(1)
C(22)	5106(3)	−3583(2)	10501(4)	4.6(1)
C(23)	4984(3)	−2714(2)	11761(4)	4.2(1)
C(24)	4505(2)	−1923(2)	11230(4)	3.4(1)
C(25)	4361(3)	−1010(2)	12481(3)	3.6(1)
C(26)	3858(2)	−260(2)	11959(3)	3.2(1)
C(27)	3466(2)	−336(2)	10106(3)	2.7(1)
C(28)	3618(2)	−1230(2)	8832(3)	2.8(1)
C(29)	4133(2)	−2021(2)	9396(3)	3.0(1)
F(30)	−757(2)	−25(1)	−3420(2)	4.0(1)
F(31)	−968(1)	1559(1)	−890(2)	3.9(1)
C(32)	116(2)	−880(2)	−1413(3)	2.7(1)
C(33)	−385(2)	−18(2)	−1733(3)	2.7(1)
C(34)	−485(2)	796(2)	−442(3)	2.7(1)
C(35)	238(2)	−1711(2)	−2735(3)	2.8(1)
C(36)	726(2)	−2587(2)	−2442(3)	3.1(1)
C(37)	−131(3)	−1803(2)	−4602(3)	3.4(1)
N(38)	1105(2)	−3312(2)	−2346(3)	4.4(1)
N(39)	−411(3)	−1944(2)	−6103(3)	5.0(1)

a) $B_{eq}=4/3\sum_i\sum_j \beta_{ij}\boldsymbol{a}_i\boldsymbol{a}_j$.

the same as that in NPY–TCNQ. The NPY molecule is more distorted from a planar structure; the dihedral angle between the pyrene and naphthalene rings is 11.6° in $(NPY)_2F_4TCNQ$.

The bond lengths in NPY are compared with those in the NPY crystal and those in the NPY–TCNQ crystal in Table 4. The hydrogen-bond structure is rather comparable to that in the NPY crystal.

The crystal stucture is shown in Fig. 4. Donors and acceptors are stacked along the a-axis. The repeat unit is considered to be NPY–F_4TCNQ–NPY. Interestingly, the overlap pattern between the NPY molecules is the same as that in NPY–TCNQ (Fig. 5(b)). The molecular overlap between NPY and F_4TCNQ is considerably different from that in the TCNQ complex. As shown in

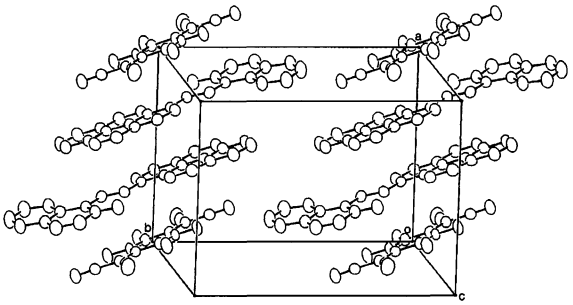

Fig. 4. Crytal structure of $(NPY)_2F_4TCNQ$.

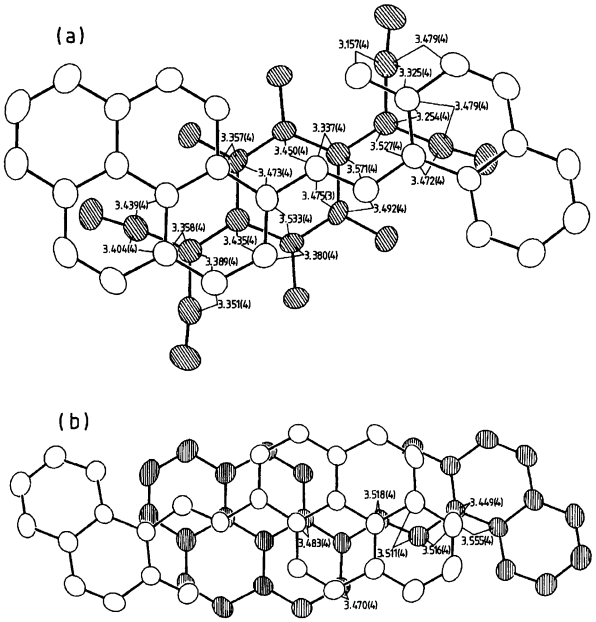

Fig. 5. Molecular overlaps between F_4TCNQ and NPY (a) and between NPY and NPY (b) in $(NPY)_2F_4TCNQ$ with short interatomic distances.

Fig. 5(a), the acceptor molecule interacts with a whole part of the donor molecule. Since only the pyrene part is nearly parallel to the F_4TCNQ molecular plane, the interplanar distances were calculated using these planes. The distance is 3.29 Å between F_4TCNQ and the pyrene ring, and is 3.46 Å between the pyrene rings. The degree of charge transfer was not estimated from the crystallographic data due to insufficiency of the data available for an estimation.

The hydrogen-bond structure in NPY–TCNQ is considerably different from that in $(NPY)_2F_4TCNQ$. The CO bond length in NPY–TCNQ suggests that the proton is bound to the nitrogen. The electron density in the hydrogen bond has been calculated from a difference Fourier synthesis using the obtained reflection data. Maps for these complexes are shown in Fig. 6. The electron density peak in NPY–TCNQ is clearly seen at the nitrogen site. In $(NPY)_2F_4TCNQ$, the electron density is broadly distributed near to the center of the hydrogen bond.

Table 4. Bond Lengths for NPY (Å)

	NPY (120 K)	NPY (295 K)	NPY–TCNQ	$(NPY)_2F_4TCNQ$
O(1)–C(3)	1.336(6)	1.319(7)	1.292(2)	1.318(4)
C(2)–C(3)	1.414(6)	1.422(8)	1.426(2)	1.418(4)
C(2)–C(11)	1.436(6)	1.430(7)	1.446(2)	1.453(4)
C(2)–C(12)	1.436(5)	1.420(6)	1.411(2)	1.418(3)
C(3)–C(4)	1.419(5)	1.401(7)	1.429(3)	1.424(4)
C(4)–C(5)	1.367(7)	1.349(9)	1.345(2)	1.351(4)
C(5)–C(6)	1.431(7)	1.434(9)	1.419(3)	1.434(4)
C(6)–C(7)	1.418(6)	1.420(8)	1.405(2)	1.410(4)
C(6)–C(11)	1.424(5)	1.412(6)	1.412(3)	1.418(3)
C(7)–C(8)	1.367(7)	1.355(10)	1.357(4)	1.364(5)
C(8)–C(9)	1.396(6)	1.356(8)	1.378(3)	1.400(4)
C(9)–C(10)	1.384(7)	1.393(9)	1.374(2)	1.373(4)
C(10)–C(11)	1.437(7)	1.424(8)	1.402(3)	1.404(4)
C(12)–N(13)	1.307(6)	1.315(7)	1.316(2)	1.314(4)
N(13)–C(14)	1.415(5)	1.410(6)	1.408(2)	1.407(3)
C(14)–C(15)	1.418(7)	1.410(8)	1.392(3)	1.401(4)
C(14)–C(27)	1.407(6)	1.390(7)	1.415(2)	1.414(4)
C(15)–C(16)	1.376(5)	1.370(7)	1.372(3)	1.386(3)
C(16)–C(17)	1.408(6)	1.387(8)	1.391(2)	1.400(4)
C(17)–C(18)	1.428(5)	1.427(6)	1.436(2)	1.434(3)
C(17)–C(28)	1.435(6)	1.426(8)	1.420(2)	1.419(4)
C(18)–C(19)	1.351(7)	1.344(9)	1.339(2)	1.346(4)
C(19)–C(20)	1.449(7)	1.458(8)	1.428(3)	1.434(4)
C(20)–C(21)	1.396(6)	1.395(8)	1.400(2)	1.399(4)
C(20)–C(29)	1.414(5)	1.400(6)	1.427(2)	1.418(3)
C(21)–C(22)	1.384(7)	1.400(9)	1.375(3)	1.383(5)
C(22)–C(23)	1.389(5)	1.367(7)	1.384(3)	1.388(4)
C(23)–C(24)	1.396(6)	1.383(8)	1.398(2)	1.400(4)
C(24)–C(25)	1.443(5)	1.431(6)	1.432(2)	1.435(4)
C(24)–C(29)	1.430(6)	1.417(8)	1.417(3)	1.420(4)
C(25)–C(26)	1.367(6)	1.354(8)	1.350(2)	1.352(4)
C(26)–C(27)	1.438(6)	1.454(8)	1.435(2)	1.443(4)
C(27)–C(28)	1.437(5)	1.433(6)	1.423(2)	1.428(3)
C(28)–C(29)	1.428(6)	1.425(7)	1.428(2)	1.425(4)
O(1)···N(13)	2.551(5)	2.530(6)	2.513(2)	2.496(3)

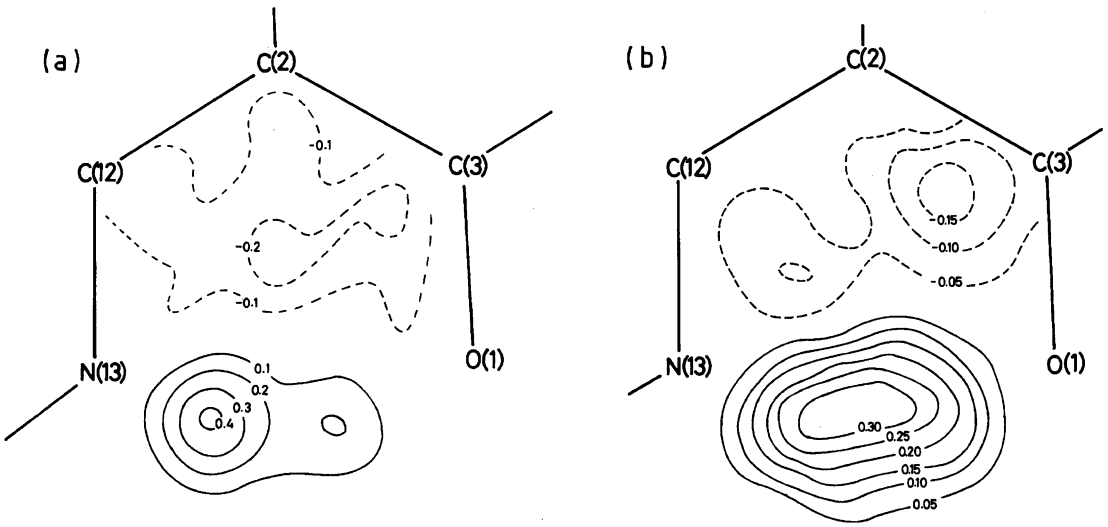

Fig. 6. Difference synthesis maps of the hydrogen-bonded chelate ring (e $Å^{-3}$) of NPY; NPY–TCNQ (a) and $(NPY)_2F_4TCNQ$ (b).

Molecular and Crystal Structures of the DNP Complexes. The atomic parameters obtained from the diffraction measurements are shown in Tables 5 and 6[6] for DNP–TCNQ and DNP–F_4TCNQ, respectively. The bond lengths in TCNQ and F_4TCNQ in these complexes are shown in Fig. 7. The bond lengths of DNP are complied in Table 7 for both complexes together with those in the single-component crystal.[1] It can again

Table 5. Fractional Coordinates ($\times 10^4$) and Equivalent Temperature Factors for DNP–TCNQ

Atom	x	y	z	B_{eq}/Å$^{2a)}$
O(1)	−1598(2)	−4124(2)	−3595(2)	4.9(1)
C(2)	−265(2)	−3413(2)	−527(3)	3.3(1)
C(3)	−427(2)	−3688(2)	−2438(3)	3.8(1)
C(4)	770(2)	−3484(2)	−3086(3)	4.2(1)
C(5)	1993(2)	−2982(2)	−1929(3)	4.1(1)
C(6)	2190(2)	−2625(2)	−12(3)	3.6(1)
C(7)	3482(2)	−2066(2)	1179(3)	4.6(1)
C(8)	3675(2)	−1744(3)	3010(4)	5.2(1)
C(9)	2577(3)	−1971(3)	3732(3)	5.0(1)
C(10)	1294(2)	−2502(2)	2615(3)	4.3(1)
C(11)	1059(2)	−2853(2)	709(3)	3.3(1)
C(12)	−1406(2)	−3718(2)	133(3)	3.6(1)
N(13)	−2621(2)	−4200(2)	−948(3)	4.0(1)
C(14)	−3803(2)	−4585(2)	−408(3)	3.7(1)
C(15)	−3799(2)	−4547(2)	1375(3)	4.1(1)
C(16)	−4999(2)	−4962(2)	−1776(3)	4.1(1)
N(17)	4647(2)	1845(2)	2425(3)	6.1(1)
N(18)	2150(2)	1456(2)	6190(3)	6.2(1)
C(19)	1167(2)	575(2)	1463(3)	2.9(1)
C(20)	−134(2)	184(2)	1772(3)	3.1(1)
C(21)	1238(2)	357(2)	−399(3)	3.1(1)
C(22)	2287(2)	1129(2)	2884(3)	3.3(1)
C(23)	3598(2)	1531(2)	2618(3)	4.1(1)
C(24)	2222(2)	1325(2)	4724(3)	4.1(1)

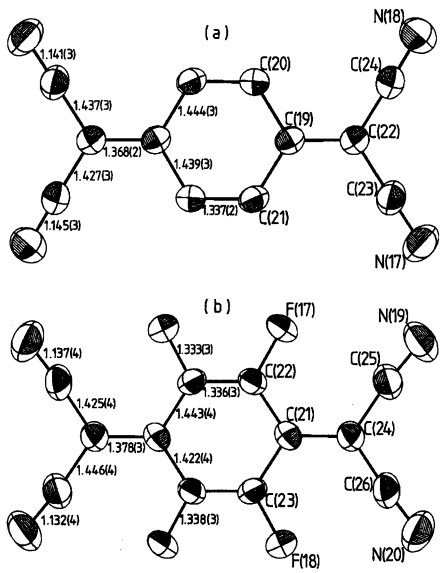

Fig. 7. ORTEP drawing and bond lengths (Å) of TCNQ in DNP–TCNQ (a) and F_4TCNQ in DNP–F_4TCNQ (b).

Table 6. Fractional Coordinates ($\times 10^4$) and Equivalent Temperature Factors for DNP–F_4TCNQ

Atom	x	y	z	B_{eq}/Å$^{2a)}$
O(1)	−1399(2)	−4136(2)	−3360(3)	6.3(1)
C(2)	−209(3)	−3379(3)	−373(4)	4.1(1)
C(3)	−262(3)	−3687(3)	−2203(4)	4.6(1)
C(4)	947(3)	−3486(3)	−2817(4)	4.9(1)
C(5)	2114(3)	−2956(3)	−1697(4)	4.8(1)
C(6)	2215(3)	−2586(3)	162(4)	3.9(1)
C(7)	3468(3)	−2019(3)	1322(4)	4.9(1)
C(8)	3567(3)	−1688(3)	3105(4)	5.5(1)
C(9)	2430(3)	−1912(3)	3789(4)	5.5(1)
C(10)	1202(3)	−2440(3)	2697(4)	4.9(1)
C(11)	1052(2)	−2804(3)	865(4)	3.9(1)
C(12)	−1391(3)	−3676(3)	265(4)	4.7(1)
N(13)	−2564(2)	−4186(2)	−846(3)	5.2(1)
C(14)	−3781(3)	−4573(3)	−352(4)	4.9(1)
C(15)	−3870(3)	−4545(3)	1360(4)	5.3(1)
C(16)	−4912(3)	−5032(3)	−1727(5)	5.5(1)
F(17)	2446(1)	484(2)	−809(2)	4.7(1)
F(18)	−340(1)	563(2)	3367(2)	4.6(1)
N(19)	4684(2)	1821(3)	2430(4)	7.2(1)
N(20)	2222(3)	1771(3)	6051(3)	7.3(1)
C(21)	1168(2)	592(2)	1403(3)	3.0(1)
C(22)	1239(2)	253(3)	−407(3)	3.2(1)
C(23)	−167(2)	286(3)	1711(3)	3.2(1)
C(24)	2259(2)	1168(3)	2762(3)	3.7(1)
C(25)	3604(3)	1511(3)	2502(4)	4.7(1)
C(26)	2198(3)	1492(3)	4580(4)	4.7(1)

Table 7. Bond Lengths for DNP (Å)

	DNP	DNP–TCNQ	DNP–F_4TCNQ
O(1)–C(3)	1.322(3)	1.290(2)	1.309(3)
C(2)–C(3)	1.408(4)	1.426(3)	1.411(4)
C(2)–C(11)	1.450(4)	1.446(3)	1.448(3)
C(2)–C(12)	1.420(4)	1.415(3)	1.427(4)
C(3)–C(4)	1.420(4)	1.442(4)	1.419(4)
C(4)–C(5)	1.342(4)	1.338(3)	1.331(4)
C(5)–C(6)	1.422(4)	1.424(3)	1.425(4)
C(6)–C(7)	1.411(4)	1.409(3)	1.415(3)
C(6)–C(11)	1.418(4)	1.419(3)	1.421(4)
C(7)–C(8)	1.350(5)	1.359(4)	1.366(5)
C(8)–C(9)	1.392(5)	1.390(4)	1.390(5)
C(9)–C(10)	1.373(4)	1.377(3)	1.368(4)
C(10)–C(11)	1.412(4)	1.411(3)	1.398(4)
C(12)–N(13)	1.305(3)	1.307(2)	1.330(4)
N(13)–C(14)	1.413(3)	1.417(3)	1.421(4)
C(14)–C(15)	1.392(4)	1.386(4)	1.385(5)
C(14)–C(16)	1.387(4)	1.386(3)	1.395(4)
C(15)–C(16)	1.383(4)	1.384(4)	1.385(5)
O(1)···N(13)	2.537(3)	2.539(3)	2.523(4)

be seen that the CO distance in the TCNQ complex is considerably short, suggesting the NH···O structure.

The crystal structures of the TCNQ and F_4TCNQ complexes are shown in Fig. 8. As can be seen from the cell parameters (Table 1), these complexes are isomorphous. The differences in the cell parameters are within 2.5%. The molecular conformation of DNP is

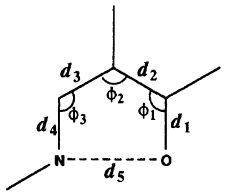

Table 8. Geometry of the Hydrogen-Bonded Chelate Ring

Compound	d_1/Å	d_2/Å	d_3/Å	d_4/Å	d_5/Å	$\phi_1+\phi_2+\phi_3$
NPY–TCNQ	1.292(2)	1.426(2)	1.411(2)	1.316(2)	2.513(2)	363.1
$(NPY)_2F_4TCNQ$	1.318(4)	1.418(4)	1.418(3)	1.314(4)	2.496(3)	362.1
DNP–TCNQ	1.290(2)	1.426(3)	1.415(3)	1.308(2)	2.539(3)	363.8
DNP–F_4TCNQ	1.309(3)	1.411(4)	1.427(4)	1.330(4)	2.523(4)	362.7
NPY (295 K)	1.319(7)	1.422(8)	1.420(6)	1.315(7)	2.530(6)	363.2
NPY (120 K)	1.336(6)	1.414(6)	1.436(5)	1.307(6)	2.551(5)	363.5
DNP	1.322(3)	1.408(4)	1.420(4)	1.305(4)	2.537(3)	363.8

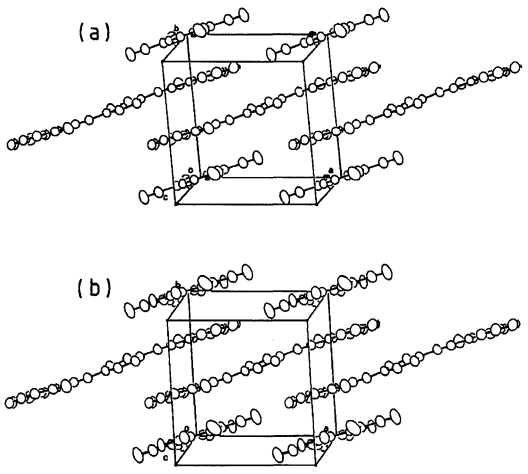

Fig. 8. Crystal Structures of DNP–TCNQ (a) and DNP–F_4TCNQ (b).

practically the same in these complexes and more planar than in the single-component crystal; the dihedral angle between the central benzene ring and the terminal naphthalene rings is 9.4° in DNP–TCNQ and is 10.2° in DNP–F_4TCNQ (21.8° in the DNP crystal). Since the DNP molecule is very long compared with TCNQ or F_4TCNQ, one DNP molecule overlaps with both TCNQ or F_4TCNQ and two other DNP molecules. The molecular overlaps are shown in Fig. 9. The acceptor molecules interact mainly with the terminal naphthalene part. The interplanar spacing is 3.30 Å in DNP–TCNQ and is 3.29 Å in DNP–F_4TCNQ. The interplanar spacing between the DNP molecules is much larger; 3.56 Å in DNP–TCNQ and 3.54 Å in DNP–F_4TCNQ. Some short interatomic distances are also indicated in Fig. 9.

The electron density in the hydrogen bond has been calculated for these two complexes; the maps are shown in Fig. 10. The electron density peak which suggests the NH structure is clearly seen in the TCNQ complex. The electron density is broadly distributed near to the center of the hydrogen bond in the F_4TCNQ complex.

The geometries of the hydrogen-bonded chelate rings are summarized in Table 8. The CO distances (d_1 in Table 8) in NPY–TCNQ and DNP–TCNQ are apparently shorter than those in the other complexes and in the single-component crystals. The N···O distance is considered to affect the equilibrium position of the hydrogen in the hydrogen bond.[8] The distances (d_5 in Table 8), especially in the TCNQ complexes, are not so much different from those in the single-component crystals. Since the crystal structure is common for the TCNQ and F_4TCNQ complexes of DNP, it is reasonable to assume that the difference in the hydrogen-bond structure arises from the difference in the strength of the charge-transfer interaction (vide infra).

Optial Spectra. The infrared spectra of the NPY complexes measured by using single-crystal specimens are shown in Fig. 11. Since the hydrogen bonds are roughly perpendicular to the molecular stacking axis in the TCNQ complex, the polarization experiments make it possible to assign the broad peak at around 2800 cm^{-1} to the NH stretching mode. The CN stretching mode of TCNQ is observed at 2214 cm^{-1}. From an empirical relation[9] between the charge on TCNQ and the frequency of the CN stretching mode, the charge on TCNQ is estimated to be about 0.3, which is consistent with the results of an X-ray analysis, in which the ground state of the complex is nearly neutral.

Since the molecular planes are not perpendicular to the stacking axis in $(NPY)_2F_4TCNQ$, the hydrogen stretching band is not clearly distinguishable by the polarization experiments. The fine structures between 2600 and 2850 cm^{-1} are observed in the spectra with light polarized parallel to the stacking axis. Although the molecular planes are not completely coincident with the polarization, the in-plane modes are expected to be more intense in the spectra with light perpendicular to the stacking axis. The bands between 2600 and 2850 cm^{-1} show an opposite tendency; the bands are weaker in the spectrum with polarization $\perp a$, though the CH stretching band is more intense in the same spectrum. These bands may be some overtones of the lower frequency modes. The ionicity of F_4TCNQ can be roughly estimated from the frequencies of the CN

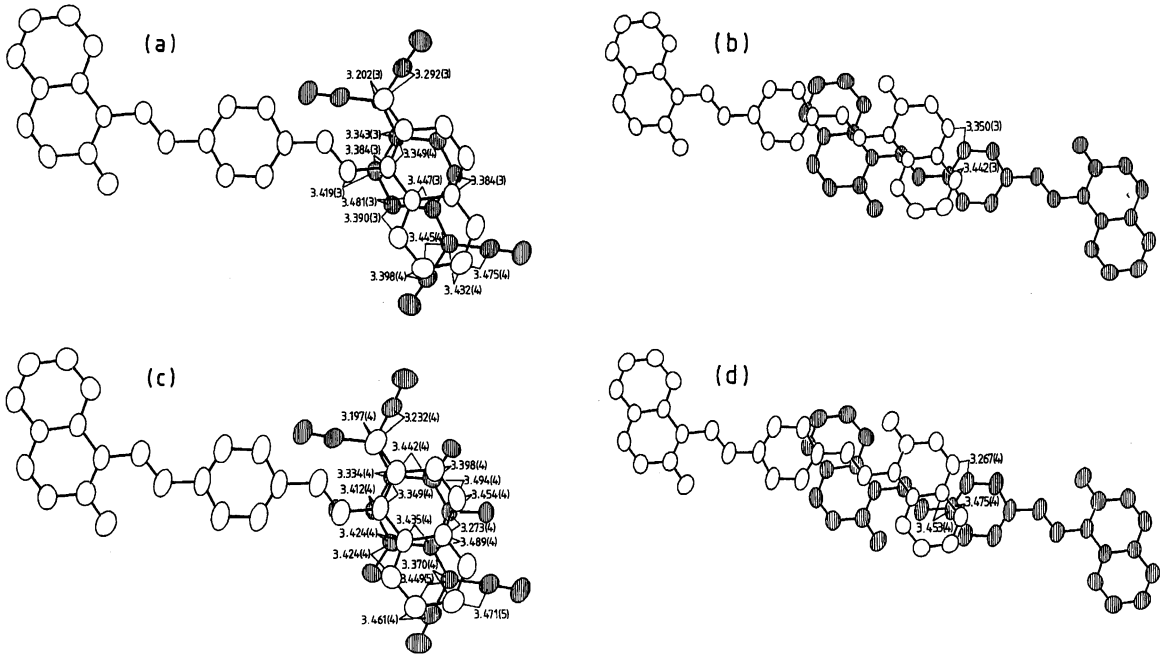

Fig. 9. Molecular overlaps between TCNQ and DNP (a) and DNP and DNP (b) in DNP–TCNQ, and between F_4TCNQ and DNP (c) and DNP and DNP (d) in DNP–F_4TCNQ.

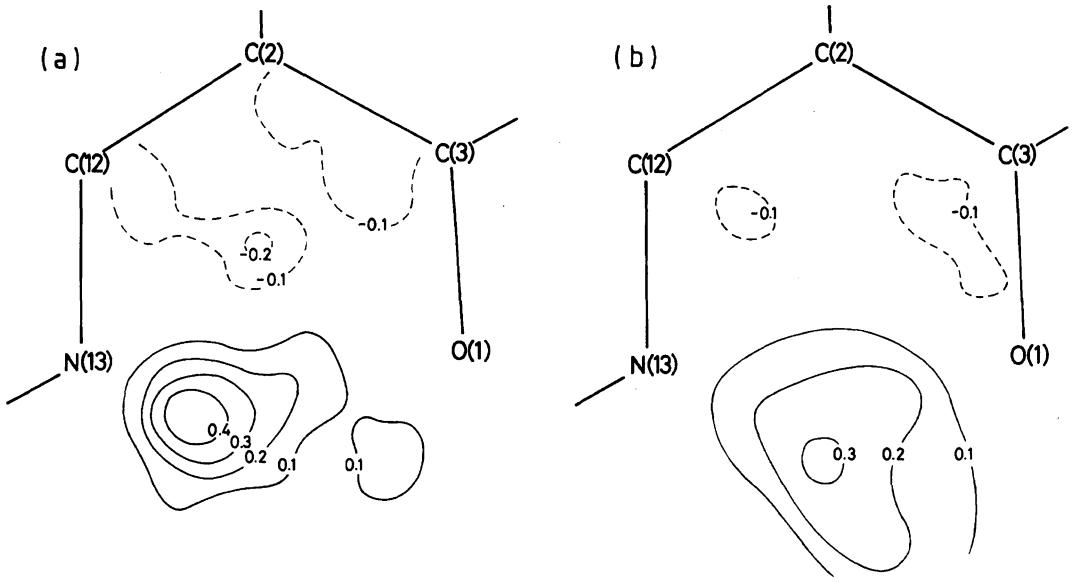

Fig. 10. Difference synthesis maps of the hydrogen-bonded chelate rings (e $Å^{-3}$) of DNP; DNP–TCNQ (a) and DNP–F_4TCNQ (b).

stretching modes.[10] Using the frequencies of the bands not only around 2200 cm^{-1}, but also in the region of 1500—1600 cm^{-1}, the charge on F_4TCNQ is estimated to be about 0.2. Considering the relatively high ionization potential of NPY, it is quite reasonable that the ground state of this complex lies in the neutral region.

The infrared spectra of the DNP complexes are shown in Fig. 12. The broad peak at around 2800 cm^{-1} of DNP–TCNQ is assignable to the NH stretching mode based on polarization experiments. The OH and/or NH stretching band in the F_4TCNQ complex has again not been clearly seen, even when using polarized light. The degree of charge transfer has been estimated to be about 0.2 for DNP–TCNQ and to be about 0.1 for DNP–F_4TCNQ based on the frequencies of the CN stretching modes. Since the oxidation potential of DNP (1.1 V vs. Ag·AgCl in acetonitrile) is slightly higher than that of NPY, it is certain that the complexes have neutral ground states.

In order to estimate the difference in the charge-transfer interaction, the visible-near-infrared spectra were measured using Nujol mull specimens. The spectra

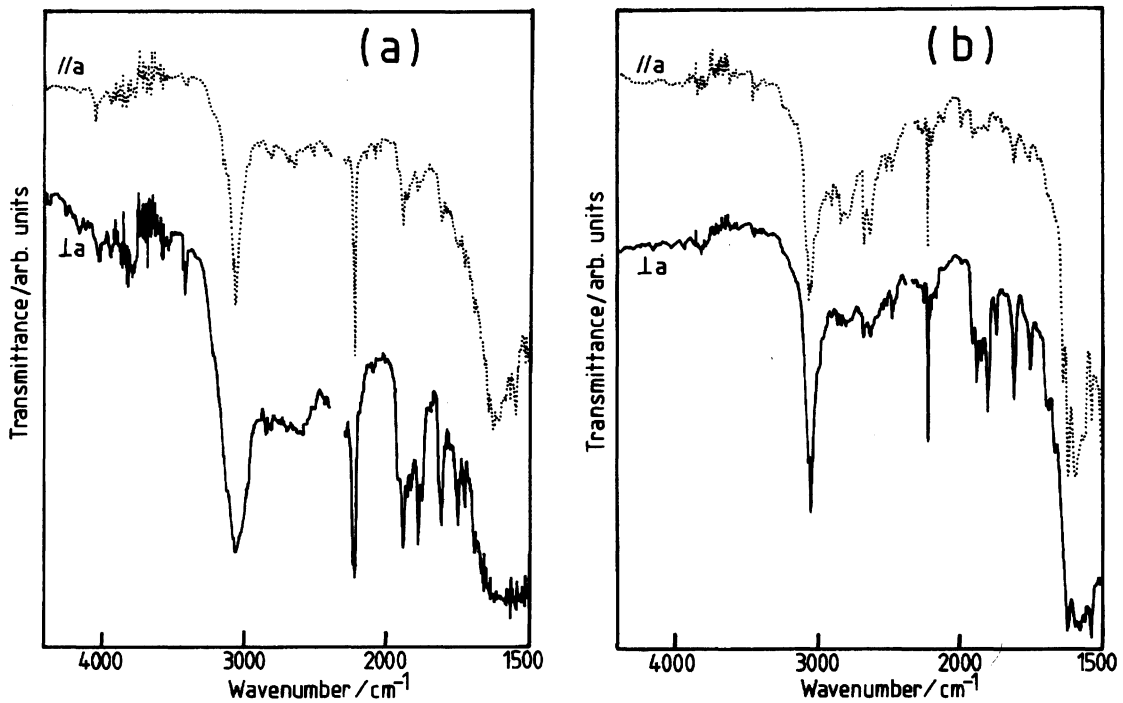

Fig. 11. Single-crystal infrared spectra for NPY–TCNQ (a) and $(NPY)_2F_4TCNQ$ (b).

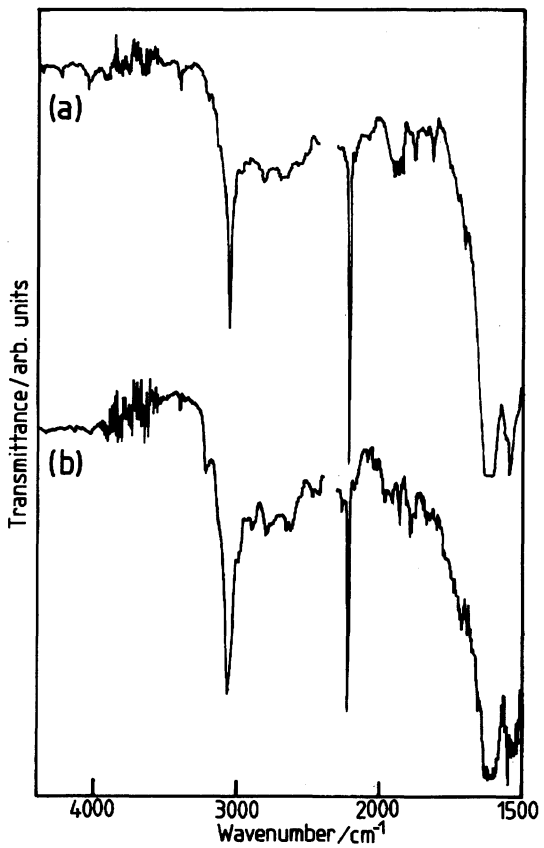

Fig. 12. Single-crystal infrared spectra for DNP–TCNQ (a) and DNP–F_4TCNQ (b).

for the NPY complexes are shown in Fig. 13. Even for a combination with a strong acceptor, F_4TCNQ, it is hardly seen the contribution from the F_4TCNQ^- species (Fig. 13(b)). The charge-transfer band lies in the near-infrared region; the peak is located at 1.27 eV for NPY–TCNQ, at 0.98 eV for $(NPY)_2F_4TCNQ$, at 1.44 eV for DNP–TCNQ, and at 1.13 eV for DNP–F_4TCNQ.

A simple relationship between the energy of charge-transfer absorption and the difference between the oxidation potential of the donor and the reduction potential of the acceptor was proposed by Torrance et al.[11] According to their model, when the complexes are in the neutral region (nearly the neutral ground state) they are linearly correlated. Figure 14(a) is a plot of the values for the complexes studied here. It can be seen that the relationships between the energy of the charge-transfer band and the difference between the oxidation potential of the donor and the reduction potential of the acceptor of these complexes obey the model proposed by Torrance et al. The complexes studied here are all in the neutral region, which is consistent with the results of the X-ray analyses and the infrared spectra.

From the above analysis, it is found that the ground states of the complexes are situated in a range far from the neutral-ionic boundary to near to the boundary. According to the distance from the boundary, the contribution from the ionic state in the ground state is scaled. Therefore, the energy of the charge-transfer band or the difference between the oxidation potential of the donor and the reduction potential of the acceptor is considered to be an index of the strength of the

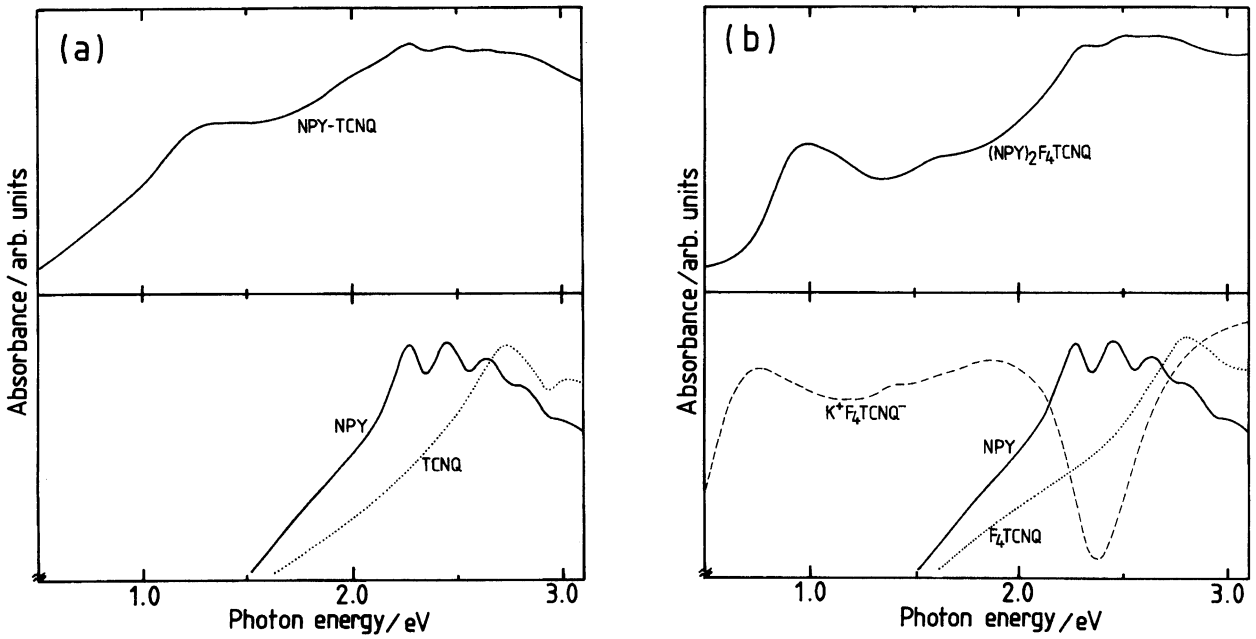

Fig. 13. Nujol mull visible and near-infrared spectra of NPY–TCNQ (a) and $(NPY)_2F_4TCNQ$ (b). Bottom spectra are for the components and a corresponding simple salt.

charge-transfer interaction. The question is whether the change in the hydrogen-bond structure is directly related to the charge transfer, and, if so, how it depends on the charge-transfer interaction. A direct comparison may be achieved by plotting the energy of the charge-transfer band and the hydrogen-bond structure. For a quantitative treatment of the hydrogen-bond structure, the CO distance is considered to be a reliable index; a plot is shown in Fig. 14(b). It can be seen that the energy of the charge-transfer band decreases monotonically with increasing CO distance. Since the change is observed in parallel with isomorphous DNP–TCNQ and DNP–F_4TCNQ, it is not due to some specific configurational interaction which arises from a difference in the crystal structure or composition. When the ground state is far from the neutral-ionic boundary, namely when the charge-transfer interaction is rather weak, the hydrogen in the hydrogen bond is distinctly bound to the nitrogen. As the ground state approaches the neutral-ionic boundary, the hydrogon is released from the nitrogen and becomes located near to the center of the hydrogen bond.

When the charge-tranfer interaction is weak, the component molecules are usually expected to have a structure in the neutral state. This means that the molecular structure is close to that in the single-component crystal. However, the hydrogen-bond structure of the complexes far from the neutral-ionic boundary is completely different from that in the single-component crystal. Since it was found that the hydrogen-bond structure in both NPY and DNP is an average between NH···O and N···HO, the energy level of the NH-form is nearly equal to that of the OH-form in the single-component crystals. Therefore, the hydrogen can be situated at both the nitrogen and oxygen sites with almost equal possibility. In TCNQ complexes, the hydrogen is completely localized at the nitrogen site. Based on the bond lengths and the difference synthesis maps related to the hydrogen bond, the energy difference between the OH- and NH-forms in the TCNQ complexes is estimated to be much larger than the thermal energy at room temperature. Therefore, the potential surface of the proton is considerably deformed by complex formation. The correlation between the hydrogen-bond structure and the CO distance suggests that the hydrogen-bond structure is changed toward an intermediate betwen the NH- and OH-forms when the charge-transfer interaction becomes stronger. In one sense, the hydrogen-bond structures in the F_4TCNQ complexes are close to that in the single-component crystals. However, it is not likely that the perturbation due to the complex formation is weaker in the F_4TCNQ complexes than in the TCNQ complexes. The charge-transfer interaction operating in the F_4TCNQ complexes is the factor that drives the hydrogen removed from the nitrogen. It is not sure, at the presnt stage, whether the final form of the hydrogen bond is intermediate between the NH- and OH-forms or not, when the complex is situated at the boundary. However, it is clear that the hydrogen in the hydrogen bond or the total hydrogen-bond structure sensitively responds to the charge-transfer interaction; a study regarding the complexes at the boundary and in the ionic region is now in progress.

In conclusion, it has been found that the hydrogen-bond structure in *N*-(2-hydroxy-1-naphthylmethylene)aniline-type compounds is sensitively changed upon

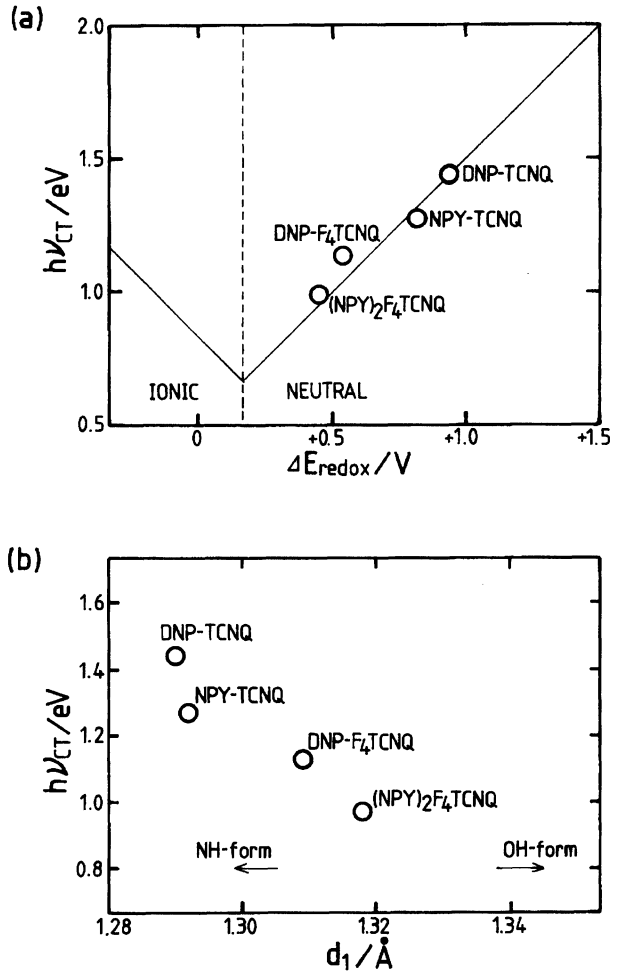

Fig. 14. Plot of the energy of charge transfer band ($h\nu_{CT}$) and the difference between the oxidation potential of the donor and the reduction potential of the acceptor (ΔE_{REDOX}). Solid-lines are from Ref. 11(a). Plot of $h\nu_{CT}$ and the CO distance (d_1 in Table 8) (b).

charge-transfer complex formation. The resultant hydrogen-bond structure is varied from the NH-form toward the structure intermediate between the NH- and OH-forms in accordance with the strength of the charge-transfer interaction, at least when the ground state is situated in some neutral range. This correlation between the hydrogen-bond interaction and the charge-transfer interaction found in this study is positive support for realization of novel materials based on the proton-electron coupling.

This work was partly supported by the Asahi Glass Foundation.

References

1) T. Inabe, I. Luneau, T. Mitani, Y. Maruyama, and S. Takeda, *Bull. Chem. Soc. Jpn.*, **67**, 612 (1994).
2) T. Inable, *New J. Chem.*, **15**, 129 (1991); T. Mitani, *Mol. Cryst. Liq. Cryst.*, **171**, 343 (1981).
3) N. Hoshino, T. Inabe, T. Mitani, and Y. Maruyama, *Bull. Chem. Soc. Jpn.*, **61**, 4207 (1988).
4) P. Main, L. Lessinger, M. M. Woolfson, G. Germain, and J. -P. Declercq, "MULTAN 78," Univ. of York, England and Louvain, Bergium (1978).
5) T. Sakurai and K. Kobayashi, *Rep. Inst. Phys. Chem. Res.*, **55**, 69 (1979).
6) The lists of sturcture factors, anisotropic thermal parameters for non-hydrogen atoms and parameters for hydrogen atoms are deposited as Document No. 67014 at the Office of the Editor of Bull. Chem. Soc. Jpn.
7) T. J. Kistenmacher, T. E. Philips, and D. O. Cowan, *Acta Crystallogr., Sect. B*, **30**, 763 (1974).
8) W. C. Hamilton and J. A. Ibers, "Hydrogen Bonding in Solids," W. A. Benjamin, Inc., New York (1976), pp. 52—55.
9) J. S. Chapell, A. N. Bloch, W. A. Bryden, M. Maxfield, T. O. Poehler, and D. O. Cohen, *J. Am. Chem. Soc.*, **103**, 2442 (1981).
10) M. Meneghetti, R. Bozio, and C. Pecile, *Synth. Met.*, **19**, 451 (1987).
11) J. B. Torrance, J. E. Vazquez, J. J. Mayerle, and V. Y. Lee, *Phys. Rev. Lett.*, **46**, 253 (1981).